Published in FUEL 90(7): 2367-2376, 2011-July

Droplet Size Distribution and Evaporation Characteristics of Fuel Spray by a Swirl Type Atomizer

[a]Tie Li, [b]Keiya Nishida, [c]Hiroyuki Hiroyasu

a Division of Energy and Environmental Systems, Hokkaido University

b Department of Mechanical System Engineering, University of Hiroshima

c Hiro Technology Brains, Inc.

Abstract

Spray atomization and evaporation play extremely important roles in mixture formation and combustion processes of direct injection (DI) gasoline engines. In this study, the fundamental characteristics of a swirl spray injected into a constant volume vessel are investigated by means of several laser diagnostic techniques including the laser diffraction-based method for droplet size distribution, the laser induced fluorescence-particle image velocimetry for velocity distributions of droplets and spray-induced ambient air flow, and the two-wavelength laser absorption-scattering technique for concentration distributions of liquid and vapor phases in the spray. The results show that the droplets at outer zone of the spray exhibit larger diameter than those at inner zone under both ambient pressures 0.1 and 0.4 MPa. While this can be partially attributed to the effect of spray-induced ambient air flow, the strength of ambient air flow become small when increasing the ambient pressure from 0.1 to 0.4 MPa, indicating the strong influence of spray dynamics on the droplet size distribution. In the evaporating spray, there are higher vapor concentrations near the spray axis than at peripheral zones. At 4.0 ms after start of injection, spray droplets almost completely evaporate under ambient temperature 500 K and pressure 1.0 MPa, but there are significantly amount of fuels with equivalence ratio below 0.5 in the spray. Reduction in ambient pressure promotes the air entrainment and droplet evaporation, but lowered ambient pressure results in more fuel vapor of equivalence ratio > 1.3 along the spray axis.

Keywords: Droplet Size Distribution; Evaporation; Swirl Spray; Direct Injection Gasoline Engines; Laser Diagnostics

1. Introduction

A further improvement of fuel efficiency in internal combustion engines is urgently required from the viewpoint of limited reserves and rising price of crude oil, and climate change due to greenhouse gas emissions. In gasoline engines, most efforts have been focused on improvements of the thermal efficiency at partial loads through unthrottled lean combustion with either stratified charge spark ignition (SI) or homogeneous charge compression ignition (HCCI).

Gasoline direct injection (DI) into cylinder can offer many advantages over port fuel injection for SI engines: improved fuel economy, enhanced transient response and startability, more precise air/fuel ratio control, reduced hydrocarbon (HC) emissions in cold-start and transient cycles, and so on [1-2]. While most improvements in fuel economy stem from the stratified charge lean combustion at partial loads due largely to unthrottled operations, preparation of the stratified charge in the vicinity of spark plug is the key challenge for the combustion system design of DISI engines because there are very limited time between the fuel injection and spark ignition, both of which must be conducted at the late stage of compression stroke.

In the first generation of production DISI engines, the stratified charge was prepared with the guidance of specially designed bowl-in-piston chamber as well as the assistance of sophisticatedly controlled in-cylinder air flow [3-4]. In the wall-guided concept, however, the relatively high particulate and HC emissions due to the spray-wall impingement are the issues, and the increased combustion chamber surface area results in extra heat transfer losses and the reduced fuel economy. Ideally, any spray-wall impingements should be avoided and a flat or shallow-dish shape combustion chamber can be used in the air- and spray-guided systems, but a well-defined spray including proper spray penetration, droplet size, and spray angle become more crucial because the mixture formation cannot be assisted by spray-piston cavity impingement [5-8]. To this purpose, a “soft” spray, which features a short penetration, a wide cone angle, a fine atomization quality and a compact structure of fuel-air mixture, would be desirable [9] , and a low-pressure high-turbulence nozzle have been proposed to generate the “soft” spray [10]. Moreover, studies by different research groups have shown that split injections can reduce spray tip penetration, promote atomization and evaporation, generate a more compact structure of combustible mixture, and enhance stability of spray ignition [11-14].

In addition to the advantages for SI engines, in-cylinder direct injection can offer extra benefits for gasoline HCCI operations. HCCI combustion can deliver both high fuel efficiency and very low soot and NOx emissions. However, most of current HCCI operations are limited to a narrow operation range, owing to the difficulties in ignition control and unacceptable pressure rise rate (PRR) at higher loads, as well as unstable operations and very high

HC/CO emissions at lower loads [15-17]. Compared to completely homogeneous operation, a stratification in either temperature or mixture distribution can moderate the PRR, reduce the HC/CO emissions, and expand the HCCI operating window [18-23]. While the stratification can be achieved by sophisticated control of intake flow [22-23], in-cylinder fuel direct injection can increase the flexibility in controls of both thermal and charge stratifications [18-21].

Although the spray atomization process is less important in DI-HCCI combustion than in DISI stratified operation, a fundamental understanding of spray atomization and mixture formation processes is necessary for optimization of engine combustion systems as well as for development of highly-reliable numerical models. With respect to the spray and mixture formation processes for DI gasoline engines, there have been a great number of papers with either experimental or numerical studies including internal flow development inside nozzles [24-27], spray atomization and evaporation in constant volume vessels [28-32], spray-ambient air interactions [33-36], spray mixture formation in optical and metal engines [37-42]. However, a comprehensive study covering the spray atomization, spray-ambient air interaction, and evaporation processes with one injection system is rarely reported, though such information would be essential to further understand the spray and mixture formation processes.

The objective of this study is to provide the comprehensive information and further understanding of the spray and mixture formation processes. *Some results that have been published in our earlier papers focused on either the spray droplet size distribution [29] or the characteristics of spray evaporation and mixture formation [30-31], and the present paper is attempted to explain how the droplet size distribution, the spray and spray inducted ambient air flows can be correlated to the characteristics of spray evaporation and mixture formation.* The paper is organized as follows: after the introduction, the experimental apparatus and conditions are described, followed by the experimental results and discussions, and finally, the major findings of this study are concluded.

2. Experimental apparatus and conditions

The instruments used in this study include the laser diffraction-based method for droplet sizing, the laser-induced fluorescence-particle image velocimetry (LIF-PIV) technique for analyzing the spray and ambient air flows, and the two-wavelength laser absorption-scattering (LAS) technique for measuring the concentrations of liquid and vapor phase sprays. Here only brief descriptions are given, and readers may find the detailed information about these techniques in [29-31, 33-34, and 43-44]. Table 1 shows a comparison of the properties between the test fuels and commercial gasoline. Dry solvent (59.5% paraffins, 0.5% olefins, 33.0% naphthenes, and 7.0% aromatics), which almost does not evaporate under atmospheric pressure and room temperature (1 atm. and 20 ºC), was

used as the test fuel in the measurements of droplet size and ambient air velocity distributions. P-xylene, which has similar physical properties to gasoline and can meet the requirement for the LAS technique, was used in the experiments of evaporating spray. Table 2 shows the experimental conditions for non-evaporating spray and Table 3 for evaporating sprays. *In all the experiments, a swirl injector of 0.5 mm hole diameter was used, and fuel was fed into the fuel accumulator, where it was separated from and pressurized by the high-pressure nitrogen gas.*

2.1 Laser diffraction-based measurements

Figure 1 shows a schematic of the experimental setup for the laser diffraction-based measurements. To obtain the droplet size information, a commercial instrument (LDSA-1400, Tonichi Computer Co.) based Fraunhofer diffraction was adopted. It is comprised of two parts: the transmitter and receiver. The transmitter includes a continuous wave helium-neon laser (wavelength: 632.8 nm, power: 2mW) and a beam collimator. After expanded and collimated into a beam of 8 mm diameter, the laser transmits the spray, and then the parallel lights are focus into a spot and the diffracted lights form a Fraunhofer diffraction pattern through the Fourier transformation lens set in the receiver. The intensity distribution of the diffracted lights at each ring of Fraunhofer pattern is captured by the annular sensors, and transferred to a computer for the size distribution analysis. *In the data analysis system, a calibration algorithm is included to minimize the effects of multiple scattering on the measuring reliability.* Because Fraunhofer diffraction pattern does not contain the spatial information of measured objects, the laser diffraction-based method can achieve merely the line-of-sight measurement of average droplet size. For spatially resolved information, a deconvolution scheme is necessary. In this study, the deconvolution algorithm proposed by Hammond [45] was used (See details in Appendix (A)).

2.2 LIF-PIV measurements

The LIF-PIV technique, which combines the features of the LIF (laser induced fluorescence) and PIV (particle image velocimetry) techniques, was employed. The PIV technique is based on measuring the displacement of particles in two pictures obtained by two-exposure imaging with a very short interval. In order to obtain a measurement of air motion, a tracer is generally necessary. In the measurements of spray-inducted air flow, the high intensity of scattered lights by spray droplets makes it very difficult to identify the scattered lights by tracer particles especially at the near or/and inside spray zones. In this study, rhodamine-B water solution was used as the tracer for the spray-induced ambient air motion. When the rhodamine-B droplets are illuminated by a laser sheet of wavelength of 532 nm, they emit the fluorescent light of wavelength (>590 nm) larger than the wavelength of the incident light. With a proper high pass filter (>560 nm), the scattered lights (532 nm) of the spray and tracer droplets can be cut off and the ambient air motion can be consequently measured from the fluorescent tracer images.

In Fig. 2, a schematic of the experimental setup for the LIF-PIV measurement is shown. The tracer injector was also a pressure-swirl one. In order to ensure the tracer droplets as small as possible, injection pressure for the tracer was set at 9.0 MPa, which is the design limit of the injector. The injection timing for the tracer was 300 ms before the start of fuel injection so that the velocity of the tracer was in the range of less than absolute 0.1 m/s at the start of fuel injection. In addition, based on the calculation of the terminal velocity, the tracing velocity of the tracer exceeding 90% of the ambient air velocity in 0.5 ms was confirmed. An Nd: YAG laser (New Wave Research Y25-20E) with cylindrical lens, which can emit two pulsed sheet lights with wavelength of 532 nm, sheet thickness of 1mm and pulse duration of 5 ns, was employed. A CCD camera (TSI PIVCAM 10-30) and a straddling method of the two pulsed lasers over the two frames of CCD camera were used to capture a pair of images. *The time intervals between the two acquired images were adjusted in a range of 5~20 microseconds for sprays and 200 microseconds for ambient air motion so as to get reasonable fuel spray and fluorescent tracer images suitable for low-noise velocity analysis.* The images were transferred to a computer, and then 2-D velocity vectors were calculated with a commercial software (INSIGHT 2.11, TSI Inc.) using a cross correlation algorithm. *The inspection window size was about 2 × 2 millimeters for both spray and ambient air flows.* Timings of the fuel and tracer injections, the laser firing, and the CCD camera shuttering were synchronized by the delay pulse generator (DG535, Stanford Research Systems).

2.3 LAS measurements

The pioneering works similar to the LAS technique can be traced to 1980s and early 1990s, in which the extinctions of visible and infrared lights were used to measure the fuel vapor/fluid concentrations [46-49]. Initially, the LAS technique using ultra-violet and visible lights was established to study the characteristics of evaporating diesel sprays [50-51], then it was developed to simultaneously and quantitatively measure the concentrations of liquid and vapor phase in an evaporating spray [30-31]. The LAS technique is based on the measurement of the relative extinction of the two wavelength (ultraviolet and visible) lights by an evaporating spray. The necessary condition is that the extinction of ultraviolet light is a result of the absorption of vapor phase and both the scattering and absorption of liquid droplets whereas the extinction of visible light is a result of only the scattering of liquid droplets, as given in Eqs. (1) and (2),

$$\ln\left(\frac{I_0}{I_t}\right)_{\lambda_A} = \ln\left(\frac{I_0}{I_t}\right)_{Lsca+Labs} + \ln\left(\frac{I_0}{I_t}\right)_{Vabs} \quad (1)$$

$$\ln\left(\frac{I_0}{I_t}\right)_{\lambda_T} = \ln\left(\frac{I_0}{I_t}\right)_{Lsca} \quad (2)$$

where I_0 and I_t are the intensities of incident and transmitted lights, respectively; λ_A and λ_T refer to the absorption wavelength (ultraviolet) and transparent wavelength (visible) lights.

According to Bohren and Huffman [52], the extinction efficiency owing to liquid droplets approximates to a constant of 2 if the droplet size is sufficiently larger than the wavelength of incident light, regardless of the wavelength of the incident light and if it is absorbed by the liquid droplets. In a dispersed cloud droplets like DI gasoline spray, the average droplet diameter is generally larger than 7 μm that can meet the above requirement. Further, it was experimentally established and described in detail in the reference [30] that the extinction efficiencies due to the liquid droplets are the same for ultraviolet and visible lights. In the experiments, the transmissivities of the ultraviolet and visible lights were measured at different positions of a non-evaporating p-xylene spray (P_a=1.0 MPa, T_a=293 K). The transmissivities agree very well for the two lights, and it was concluded that while the extinction of ultraviolet light is owing to both absorption and scattering of liquid droplets, the extinction owing to absorption is negligibly small compared with that caused by scattering. Therefore, from the extinction difference between the ultraviolet and visible lights, the vapor concentration distribution can be obtained according to the Lambert-Beer's law, Eq. (3),

$$\ln\left(\frac{I_0}{I_t}\right)_{Vabs} = \ln\left(\frac{I_0}{I_t}\right)_{\lambda_A} - \ln\left(\frac{I_0}{I_t}\right)_{\lambda_T} = \int_0^L \frac{\varepsilon}{MW} \cdot C_v dl \quad (3)$$

Where ε is the molar absorption coefficient, MW the molecular weight and C_v the vapor concentration. Moreover, based on the light scattering theory by small particles, the definition equation of Sauter mean diameter (SMD) and the fuel injection rate, the liquid phase concentration can be obtained.

Because the LAS technique is a line-of-sight measurement, some assumptions have to be made to obtain the local fuel concentration. First, the spray is assumed to be axially symmetric. Then the cross section of the spray is divided by a number of small rings with a width of 0.663 mm, and in each ring the vapor and liquid droplets are assumed to be homogeneously distributed. Finally, the local fuel concentrations of the line-of-sight measurements are deconvoluted by employing an 'onion-peeling' model and expressed in terms of equivalence ratios of both liquid and vapor phases. *The equivalence ratios are defined by the actual fuel-air ratio in the ring divided by the stoichiometric ratio of the fuel. A flow chart of the data acquisition and processing procedure can be found in Appendix (B).*

In order to have an estimation of the overall accuracy of the LAS measurement, the experiments of completely

evaporated spray were conducted. The total mass of vapor over the completely evaporated spray measured by LAS was compared with the fuel injection quantity measured by a weighting method. The LAS measurements show relative errors less than 8% when the total injection quantity is more than *5.0 mg*.

Figure 3 shows a schematic of the experimental setup for the LAS measurement. In this study, a Nd:YAG laser (Continuum NY61-10), which can provide both ultraviolet (wavelength 266 nm) and visible (532 nm) lights, was used as the light sources. The ambient temperature and pressure were 500 K and 1.0 MPa, respectively. In the investigations of the effects of ambient pressure, it was changed from 0.5 to 1.5 MPa in 0.5 MPa increments. Fuel temperature was kept constant at about 20 °C with coolant.

3. Results and discussion

3.1 Droplet size distribution

Figure 4 shows the Mie scattering images of the spray droplets by a laser sheet method with the experimental setup similar to that in Fig. 2 at 1.5, 2.0 and 3.0 ms after start of injection (ASOI) under ambient pressures 0.1 and 0.4 MPa. The spray shows a wide-cone structure at 0.1 MPa and narrow-cone under elevated ambient pressure. *The dominant reason for the narrowed cone of spray under elevated ambient pressure could be the higher ambient resistance causing droplets lose more quickly their momentum, while the influence of spray-induced ambient air flow might be to some extent another explanation.* Noteworthy is that in the spray under ambient pressure 0.1 MPa, two counter-vortex structures can be identified at about 20 mm downstream from the injector tip at 1.5 ms, and they move downward with the spray penetration. Under the higher ambient pressure, there are also two vortex-like structures, but they tend to extend the body length rather than moving down of the whole structure with the spray penetration.

Figure 5 shows the temporal variations of SMD and DV90 by the line-of-sight measurements. SMD is an average droplet diameter containing the information about the volume to surface ratio of the entire measured droplets, and DV90 is a droplet diameter such that 90% of total liquid volume (or mass) is in droplets of smaller diameter [53]. Both SMD and DV90 are extremely important parameters in the spray and mixture formation processes for DI gasoline engines. Under ambient pressure 0.1 MPa, both the SMD and DV90 decrease with time proceeding. Under ambient pressure 0.4 MPa, however, these two parameters experience a decrease and then increase up to a larger value. As shown in Fig. 4, under ambient pressure 0.4 MPa, the line-of-sight measuring volume just passes through the spray leading edge at 1.5 ms. The droplets at the spray leading edge with high penetrating velocity at early time could have encountered stronger resistant force by the ambient air under the higher ambient pressure,

resulting in relatively fine atomization. At 3.0 ms, the measured droplets locate at middle stream of the spray, and they would subject to the strong effects of the spray-induced vortex-like air flow moving small droplet into the center zone. These small droplets might penetrate downward with high velocity air flows, resulting in the relative large droplet size at middle stream of the spray, but further works need to be done to make this issue clearer.

Figure 6 (a) shows the spatial droplet size distributions at 1.5, 2.0 and 3.0 ms under ambient pressure 0.1 MPa. Generally, the droplets at outer zone of the spray exhibit larger diameter than those at inner zone. This is in a good agreement with the characteristics of 'hollow cone' spray generated from swirl injectors [1-2]. Referring to the spray images shown in Fig. 4, one may also obtain an explanation that this could be a combined result of spray dynamics and spray-ambient air interactions, which will be further discussed in Section 3.2. While at the zones far from the spray axis, the deconvoluted diameters show almost the same value as the line-of-sight ones, there show significant differences between the deconvoluted and line-of-sight diameters at the zones near spray axis *at 1.5 ASOI, but no significant differences can be found at 2.0 and 3.0 ms.* Figure 6 (b) shows the spatial droplet size distributions at 3.0 ms under ambient pressure 0.4 MPa. Here the data at 1.5 and 2.0 ms are not shown, owing to the too narrow spray. As expected, the droplets at the zones far from the spray axis show two times greater diameter than those at near spray axis zones. *This can be attributed to the fact that the induced air flow could take the relatively small droplets into the center zones while leave the relatively large droplets remaining at the peripheral zones. In addition, the dynamics of the swirling spray may be another explanation; that is, the centrifugal force may lead to larger droplets locating at outer zones and smaller droplets at the center zones.* At the zones near spray axis, the deconvoluted results show merely a little smaller diameter than the line-of-sight measurements. This can be attributed to the fact that there could be much higher density of very small droplets near the spray axis than at the peripheral zones such that these small droplets dominated the SMD calculation in the line-of-sight measurements.

3.2 Velocity distributions of spray droplets and ambient air flow

Figure 7 shows the velocity distributions of spray droplets and spray-induced ambient air flow at 3.0 ms ASOI under two ambient pressures (a) 0.1 and (b) 0.4 MPa. Here the velocity distribution of spray droplets was obtained by the PIV measurement using a pair of Mie scattering images of the droplets, while that of ambient air flow by the LIF-PIV measurement using a pair of fluorescent images of tracer particles. One may note that velocity vectors at some location are missing in the sprays. This is a result that a threshold was set to cut off some unreasonably high velocity vectors owing to the uncertainties in the PIV measurements in the high density zones of spray droplets.

Under ambient pressure 0.1 MPa, while two vortex-like structures can be found for both the spray droplets and

ambient air flow, the vortex structures of the ambient air flow locate about 5 mm upstream compared with those of spray droplets. *This discrepancy in the location of vortex-like flow was also found in the earlier work [33-34], and it might be due to the difference between the penetrating velocities of spray and induced air flow.* Strong air entrainment into the spray occurs at the spray tail zones, while there are the highest velocity at the center zones between the two vortex structures for both droplets and ambient air. In addition, zones near the spray axis show significantly greater velocity than peripheral zones. Under ambient pressure 0.4 MPa, the vortex-like structures can also be found with careful examination of the velocity vectors for both the spray droplets and ambient air, but the flow strengths are smaller and the vortex structures are closer to the spray axis than those under ambient pressure 0.1 MPa. The air entrainment at the spray tail zones is also dominant under ambient pressure 0.4 MPa. The spray droplets show the highest velocity at the middle stream near the spray axis, and this supports well the above discussion regarding to Fig. 5(b). However, there show very low velocity of ambient air flow at the same zones. A reasonable explanation cannot be reached for this discrepancy at present and further investigations are necessary to address this issue.

The spray dynamics and the ambient air flow would play very important roles in the droplet secondary break-up and droplet size distribution as have been shown in Section 3.1, and further these would influence greatly on the mixture concentration distribution that will be discussed in the next section.

3.3 Concentration distributions of liquid and vapor phase sprays

Figure 8 shows the temporal variations of liquid and vapor phase equivalence ratio (ϕ) distributions in the spray. The left hand side of the image at each time shows the liquid phase and the right hand side shows the vapor phase. At 1 ms ASOI, in the liquid phase, an initial spray is clearly found at 20-30 mm downstream the injection tip and almost no evaporation occur due to the relatively short time. At 2 ms, the liquid initial spray gradually disappears, but it does not show significantly higher vapor concentrations than the main spray. This may be attributed to the fact that the poorly atomized initial spray broke up and formed a droplet cluster under the high ambient pressure conditions, and vaporized and mixed quickly with the ambient hot gas, owing to the relatively low droplet number density [29]. In the main spray, the highest equivalence ratio of vapor does not distribute in the near axial zones, but at some distance from the spray axis. This could be attributed to the influence of the vortex flows as have been discussed in Section 3.2. At 3.0 ms, there is more liquid fuel at the spray leading edge, and similar phenomena can also be found in the Mie scattering image of non-evaporating spray in Fig.4. This may be attributed to the fact that droplets at the leading edge broke up and lose the moments, and as a result, they collided and coalesced with the

coming droplets with high velocity from upstream. At 4.0 ms, the liquid phase fuel decreases gradually and the vapor phase fuel distributes more extensively. Noteworthy is that the vapor phase spray penetrates along the axial direction, but not so much along the radial direction. This may be attributed to the fact that the vapor phase is affected more easily by the ambient air flow, and the air entrainment under the high ambient pressure suppresses the air motion along radial direction.

Figure 9 shows the equivalence ratios of (a) liquid and (b) vapor phases along radial direction from the spray axis at 25 mm downstream of the injector tip. At 1.0 ms, the equivalence ratio of liquid phase shows a rather high value near the spray axis, owing to the initial spray. With evaporation proceeding, the equivalence ratio of liquid phase decreases, and the equivalence ratio of vapor phase increases gradually. Interestingly, the peak of the equivalence ratio of vapor phase locates some distance from the spray axis, especially at 2.0 and 3.0 ms. This can be attributed to the influence of the vortex-like ambient air flow. At 4.0 ms, most liquid droplets have evaporated, and the relatively high equivalence ratio of vapor shifts to zones near the spray axis.

Figure 10 shows the temporal variations of probability density function (PDF) of equivalence ratio in the (a) liquid and (b) vapor phase sprays. As expected, the liquid decreases and the vapor increases in the spray with time proceeding; at 4.0 ms, about 80% of the fuel has evaporated, and the left liquid phase distributes with very low equivalence ratio. Noteworthy is that while a large amount of vapor phase fuel distributes in the range of equivalence ratio from 0.5 to 1.2, there are about 39% of fuel in vapor phase with equivalence ratio below 0.5. These 'over lean' mixture should be avoided because it could be one of sources of HC emissions in DISI engines.

Figure 11 shows the effect of ambient pressure on the spatial equivalence ratio distributions of liquid and vapor phases, and Figure 12 shows the effect of ambient pressure on the mass of liquid, vapor and entrained air in the spray, at 3 ms ASOI. *With the ambient pressure decreasing, the spray penetration distance in either radial or axial direction becomes longer as shown in Fig. 11, the quantity of entrained hot air increases, and the spray evaporation is promoted as shown in Fig. 12. This agrees well with the analysis of the effects of ambient pressure on the spray-induced ambient air flow in Section 3.2. In addition, as have been shown in Fig. 6, the droplet size could be smaller under the lower ambient pressure, which would also contribute to some degree to the faster fuel evaporation. However, it should be noted that under ambient pressure 0.5 MPa, there are significant amount of vapor phase fuel with equivalence ratio above 1.3 along the spray axis as shown in Fig. 11*, as a balanced result between the evaporation and fuel-air mixing rates.

4. Conclusions

The droplet size distribution, the velocity distributions of droplet and ambient air flows, and the concentration distributions of liquid and vapor phases in the swirl spray have been studied. The major findings are summarized as follows:

- The droplets at the peripheral zones exhibit greater diameter than those near the spray axis under both ambient pressures 0.1 and 0.4 MPa. While this can be partially attributed to the effect of spray-induced ambient air flow, the strength of ambient air flow become small when increasing the ambient pressure from 0.1 to 0.4 MPa, indicating the strong influence of spray dynamics on the droplet size distribution.
- Though the diameter of droplets at the center zones is smaller, the number density is significantly higher than at the peripheral zones.
- Two counter-rotating vortex-like ambient air flows can be found at middle stream of the spray, but strong air entrainments into the spray occur mainly at the spray tail zones, under both ambient pressures 0.1 and 0.4 MPa.
- In the evaporating spray, there are higher vapor concentrations near the spray axis than at peripheral zones. At 4.0 ms after start of injection, spray droplets almost completely evaporate under ambient temperature 500 K and pressure 1.0 MPa, but there are significantly amount of fuels with equivalence ratio below 0.5 in the spray.
- Reduction in ambient pressure promotes the air entrainment and droplet evaporation, but lowered ambient pressure results in more vapor of equivalence ratio > 1.3 along the spray axis, as a balanced result between the evaporation and fuel-air mixing rates.

Acknowledgement

The authors wish to acknowledge the assistances of Mr. D. Takaki and Mr. T. Onoe, the former graduate students of the Graduate School of Engineering, University of Hiroshima, in the experiments. This study was partially supported by Mazda Motor Corporation.

Reference

[1] Zhao FQ, Lai MC, Harrington DL. Automotive spark ignited direct-injection gasoline engines. Prog Energy Combst Sci 1999; 25(5): 437–562.

[2] Zhao FQ, Harrington DL, Lai MC. Automotive gasoline direct-injection engines. Society of Automotive Engineering, Inc; 2002.

[3] Iwamoto Y, Noma K, Nakayama O, Yamauchi T, Ando H. Development of gasoline direct injection engine. SAE Paper 1997; 970541.

[4] Harada J, Tomita T, Mizuno H, Mashiki Z, Ito Y. Development of direct injection gasoline engine. SAE Paper 1997; 970540.

[5] Cathcart G, Zavier C. Fundamental Characteristics of an air-assisted direct injection combustion system as applied to 4-stroke automotive gasoline engines. SAE Paper 2000; 2000-01-0256.

[6] VanDerWege BA, Han Z, Iyer CO, Munoz RH, Yi J. Development and analysis of a spray-guided DISI combustion system concept. SAE Paper 2003; 2003-01-3105.

[7] Katashiba H, Honda T, Kawamoto M, Sumida M, Fukutomi N, Kawajir K. Improvement of center injection spray guided DISI performance. SAE Paper 2006; 2006-01-1001.

[8] Yamamoto S, Tanaka D, Sato K, Yokoe M. Keys to understanding spray-guided combustion of a narrow-spacing gasoline direct injection SI engine with a centrally-mounted multi-hole injector. SAE Paper 2009; 2009-01-1497.

[9] Yang J, Kenney T. Some concepts of DISI engine for high fuel efficiency and low emissions, SAE Paper 2002; 2002-01-2747.

[10] Xu M, Porter D, Daniels C, Panagos G, Winkelman J. Soft spray formation of a low-pressure high-turbulence fuel injector for direct injection gasoline engines. SAE Paper 2002; 2002-01-2746.

[11] Li T, Nishida K, Zhang Y, Onoe T, Hiroyasu H. Enhancement of stratified charge for DISI engines through split injection (Effect and its mechanism). JSME Inter J (B) Fluid Thermal Eng 2005; 48(4): 687-694.

[12] Li T, Nishida K, Zhang Y, Hiroyasu H. Effect of split injection on stratified charge formation of direct injection spark ignition engines. Inter J Engine Research 2007; 8(2): 205-219.

[13] Mitroglou N, Nouri JM, Arcoumanis C. Spray structure from double fuel injection in multi-hole injectors for gasoline direct-injection engines. Atomization Sprays 2009; 19(6): 529-545.

[14] Sauter W, Pfeil J, Velji A, Spicher U, Laudenbach N, Altenschmidt F, Schaupp U. Application of Particle Image Velocimetry for Investigation of Spray Characteristics of an Outward Opening Nozzle for Gasoline Direct Injection. SAE Paper 2006; 2006-01-3377.

[15] Zhao F et al. ed. Homogeneous charge compression ignition (HCCI) engines: key research and development issues. Society of Automotive Engineering, Inc; 2003.

[16] Dec JE. Advanced Compression-ignition engines – understanding the in-cylinder processes. Proc Combst Inst 2009; 32: 2727-2742.

[17] Yao M, Zheng Z, Liu H. Progress and recent trends in homogeneous charge compression ignition (HCCI) engines. Prog Energ Combst Sci 2009; 35: 398-437.

[18] Dec JE, Sjöberg M. A parametric study of HCCI combustion – the sources of emissions at low loads and the effects of GDI fuel injection. SAE Paper 2003; 2003-01-0752.

[19] Aroonsrisopon T, Werner P, Sohm VM, Foster DE, Ibara T, Morikawa T, Iida M, Waldman JO. Expanding the HCCI operation with the charge stratification. SAE Paper 2004; 2004-01-1756.

[20] Dec JE, Hwang W, Sjöberg M. An investigation of thermal stratification in HCCI engines using chemiluminescence imaging. SAE Paper 2006; 2006-011518.

[21] Hwang W, Dec JE. Fuel stratification for low-load HCCI combustion: performance & fuel-PLIF measurements. SAE Paper 2007; 2007-01-4130.

[22] Kakaho A, Nagamine M, Amenomori Y, Urushihara T, Itho T. In-cylinder temperature distribution measurement and its application to HCCI combustion. SAE Paper 2006-01-1202.

[23] Herold RE, Ghandhi JB. Investigation of bulk in-cylinder stratification with split intake runners. SAE Paper 2007-01-4044.

[24] Abo-Serie E, Arcoumanis C, Gavaises M. Pressure-swirl atomizers for DISI engines: further modeling and experiments. SAE Paper 2000; 2000-01-1044.

[25] Cousin J, Nuglisch HJ. Modeling of internal flow in high pressure swirl injectors. SAE Paper 2001; 2001-01-0963.

[26] Papoulias D, Giannadakis E, Mitrolou N, Gavaises M, Theodorakakos A. Cavitation in fuel injection systems for spray-guided direct injection gasoline engines. SAE Paper 2007; 2007-01-1418.

[27] Nouri JM, Mitroglou N, Yan Y, Arcoumanis C. Internal flow and cavitation in a multi-hole injector for gasoline direct-injection engines. SAE Paper 2007; 2007-01-1405.

[28] Nouri JM, Whitelaw JH. Spray characteristics of a gasoline direct injector with short durations of injection. Experiments in fluids 2001; 31(4): 377-383.

[29] Li T, Nishida K, Hiroyasu H. Characterization of initial spray from a DI gasoline injector by holography and laser diffraction method. Atomization Sprays 2004; 14(5): 477-494.

[30] Yamakawa M, Takaki D, Li T, Zhang Y, Nishida K. Quantitative measurement of liquid and vapor phase concentration distributions in a DI gasoline spray by the laser absorption scattering (LAS) technique. SAE Trans J Engine 2002; 111(3): 2194-2206.

[31] Li T, Yamakawa M, Takaki D, Nishida K, Zhang Y, Hiroyasu H. Characterization of mixture formation processes in DI gasoline sprays by the laser absorption and scattering (LAS) technique – effect of injection condition. SAE Trans Fuels Lubricants 2003; 112(4): 1115-1124.

[32] Nauwerck A., Pfeil J, Velji A, Spiche r U, Richter B. A basic experimental study of gasoline direct injection at significantly high injection pressures. SAE Paper 2005; 2005-01-0098.

[33] Yamakawa M, Isshiki T, Yoshizaki T, Nishida K. Measurement of ambient air motion of DI gasoline spray by LIF-PIV. Proc. 5th COMODIA 2001; 5: 499-504.

[34] Lee J, Nishida K. Simultaneous Flow Field Measurement of D.I. Gasoline Spray and Entrained Ambient Air by LIF-PIV Technique. SAE Paper 2003; 2003-01-1115.

[35] Choi J, Lee S, Bae C. Spray and flow-field interaction of gasoline direct injection. Atomization Sprays 2004; 14(2): 159-174.

[36] Nouri JM, Whitelaw JH. Gasoline sprays in uniform crossflow. Atomization Sprays 2007; 17(7): 621-640.

[37] Kubach H, Gindele J, Spicher U. Investigations of mixture formation and combustion in gasoline direct injection engines. SAE Paper 2001; 2001-01-3647.

[38] Davy M, Williams P, Anderson R. Effects of fuel composition on mixture formation in a firing direct-injection spark-ignition (DISI) engine: an experimental study using Mie-scattering and planar laser-induced fluorescence (PLIF) technique. SAE Paper 2000; 2000-01-1904.

[39] Kakuho A, Yamaguchi K, Hashizume Y, Urushihara T, Itoh T, Tomita E. A study of air-fuel mixture formation in direct-injection SI engines, SAE Trans J Fuels Lubricants 2004; 113(4):1169-1180.

[40] Fischer J, Velji A, Spicher U, Zimmermann F, Schulz C. Measurement of the equivalence ratio in the spark gap region of a gasoline direct injection engine with spark emission spectroscopy and tracer-LIF. SAE Paper 2004; 2004-01-1916.

[41] Kim S, Nouri JM, Yan Y, Arcoumanis C. Effects of intake flow on the spray structure of a multi-hole injector in a DISI engine. Inter J Auto Tech 2009; 10(3): 277-284.

[42] Lindagren R, Denbratt I. Influence of wall properties on the characteristics of a gasoline spray after wall impingement. SAE Paper 2004; 2004-01-1951.

[43] Bachalo WD. Spray diagnostics for the twenty-first century. Atomization Sprays 2000; 10: 439-474.

[44] Gulder OL. Multiple scattering effects in dense spray sizing by laser diffraction. Aerosol Sci Tech 1990; 12: 570-577.

[45] Hammond DC. Deconvolution technique for line-of-sight optical scattering measurements in axisymmetric sprays. Applied Optics 1981; 20(3): 493-499.

[46] Chraplyvy AR. Non-intrusive measurements of vapor concentrations inside sprays. Applied Optics 1981; 20(15): 2620-2624.

[47] Gougeon P, Le Toulouzan NJ, Gouesbet G, Thenard C. Optical diagnosis in multiple scattering media using a visible infra-red double extinction technique. J Phys E 1987; 20: 1235-1242.

[48] Drallmeier JA, Peters RE. Experimental investigation of fuel spray vapor phase characterization. Atomization Sprays 1991; 1: 63-88.

[49] Billings TP, Drallmeier JA. A detailed assessment of the infrared extinction technique for hydrocarbon vapor measurements in a controlled two-phase flow. Atomization Sprays 1994; 4: 99-121.

[50] Suzuki S, Nishida K, Hiroyasu H. Simultaneous concentration measurement of vapor and liquid in an evaporating diesel spray. SAE Paper 1993; 930863.

[51] Zhang Y, Nishida K, Yoshizaki T. Quantitative measurement of droplets and vapor concentration distributions in diesel sprays by processing UV and visible images. SAE Paper 2001; 2001-01-1294.

[52] Bohren EE, Huffman DT. Absorption and scattering of light by small particles. New York: Wiley-Interscience; 1988.

[53] Lefebvre AH. Atomization and sprays. Hemisphere Pub; 1988.

Caption of tables

Table 1
Fuel properties

Fuel property	unit	Gasoline	Dry solvent	p-xylene
Boiling point	K	$348 \leq T_{50} \leq 383$[a]	$T_{50} \leq 453$	412
Density[b]	kg/cm^3	≤783	773	857
Kinetic viscosity[b]	mm^2/s	0.737[c]	0.926	0.706
Surface tension[b]	mN/m	20.8[c]	24.5	27.8

a T_{50}: 50% distillation temperature
b under standard conditions
c iso-octane

Table 2
Experimental conditions for non-evaporating spray

Fuel	Dry solvent
Injection pressure	5.0 MPa
Injection duration/mass	0.9 ms/6.0 mg
Ambient temperature	300 K
Ambient pressure	0.1 and 0.4 MPa

Table 3
Experimental conditions for evaporating spray

Fuel	p-xylene
Injection pressure	5.0 MPa
Injection duration/mass	0.9 ms/6.0 mg
Ambient temperature	500 K
Ambient pressure	0.5, 1.0 and 1.5 MPa

Caption of figures

Fig.1 Experimental setup for measurement of spray droplet size distribution

Fig. 2 Schematic of experimental apparatus for LIF-PIV and laser sheet imaging

Fig. 3 Schematic of experimental apparatus for LAS measurement

Fig. 4 Mie scattering images of spray droplets by laser sheet method (T_a = 300 K, Fuel: dry solvent) (a) P_a = 0.1 MPa. (b) P_a = 0.4 MPa

Fig.5 Temporal variations of SMD and DV90 (T_a = 300 K, Fuel: dry solvent, r = 0 mm, z = 30 mm) (a) P_a = 0.1 MPa (b) P_a = 0.4 MPa

Fig.6 Spatial droplet size distribution (T_a = 300 K, Fuel: dry solvent, r = 0 mm, z = 30 mm) (a) P_a = 0.1 MPa (b) P_a = 0.4 MPa

Fig. 7 Velocity distributions of spray droplets and spray-induced ambient air flow (T_a = 300 K, t = 3 ms ASOI, Fuel: dry solvent) (a) P_a = 0.1 MPa (b) P_a = 0.4 MPa

Fig. 8 Temporal variations of spatial equivalence ratio distributions of liquid and vapor phases in the spray (T_a = 500 K, P_a = 1.0 MPa, Fuel: p-xylene)

Fig. 9 Temporal variations of equivalence ratio distributions along radial direction from spray axis (T_a = 500 K, P_a = 1.0 MPa, Fuel: p-xylene, *z*=25 mm) (a) liquid phase; (b) vapor phase

Fig. 10 *Temporal variations of probability density function (PDF) of equivalence ratio in the (a) liquid and (b) vapor phase sprays* (T_a = 500 K, P_a = 1.0 MPa, Fuel: p-xylene)

Fig. 11 Effect of ambient pressure on spatial equivalence ratio distributions of liquid and vapor phases in the spray (T_a=500 K, t = 3 ms ASOI, Fuel: p-xylene)

Fig. 12 Effect of ambient pressure on mass of liquid, vapor and entrained air in the spray (T_a=500 K, t = 3 ms ASOI, Fuel: p-xylene)

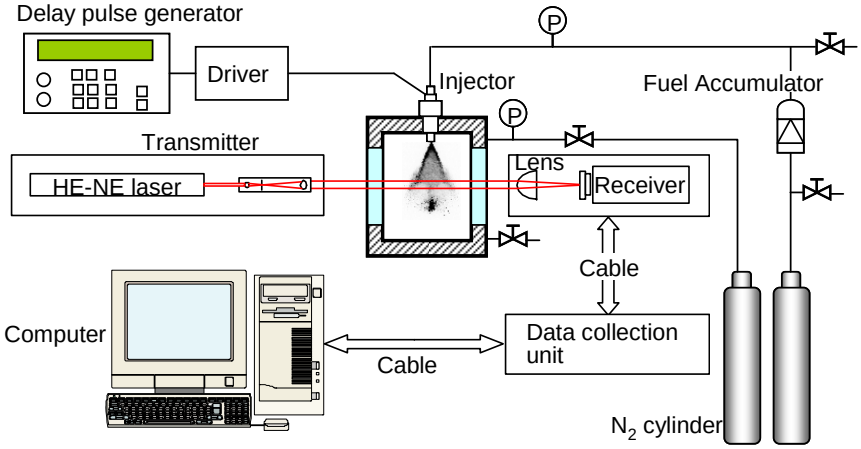

Fig.1 Experimental setup for measurement of spray droplet size distribution

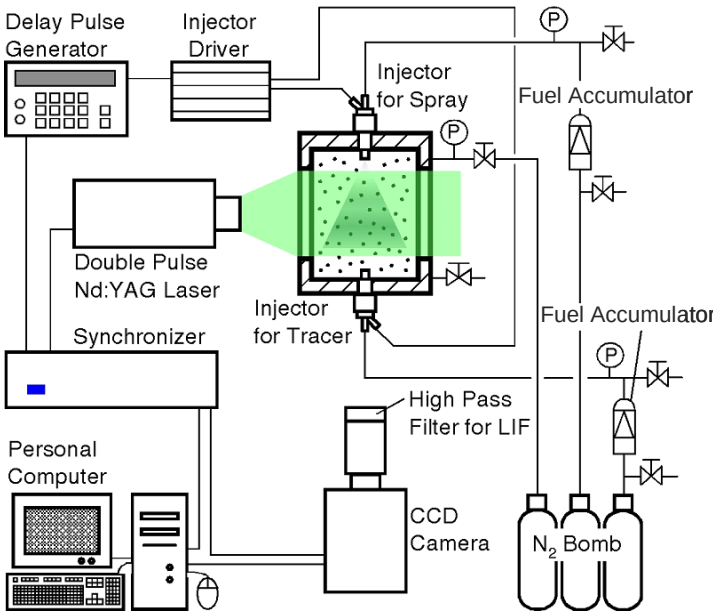

Fig. 2 Schematic of experimental apparatus for LIF-PIV and laser sheet imaging

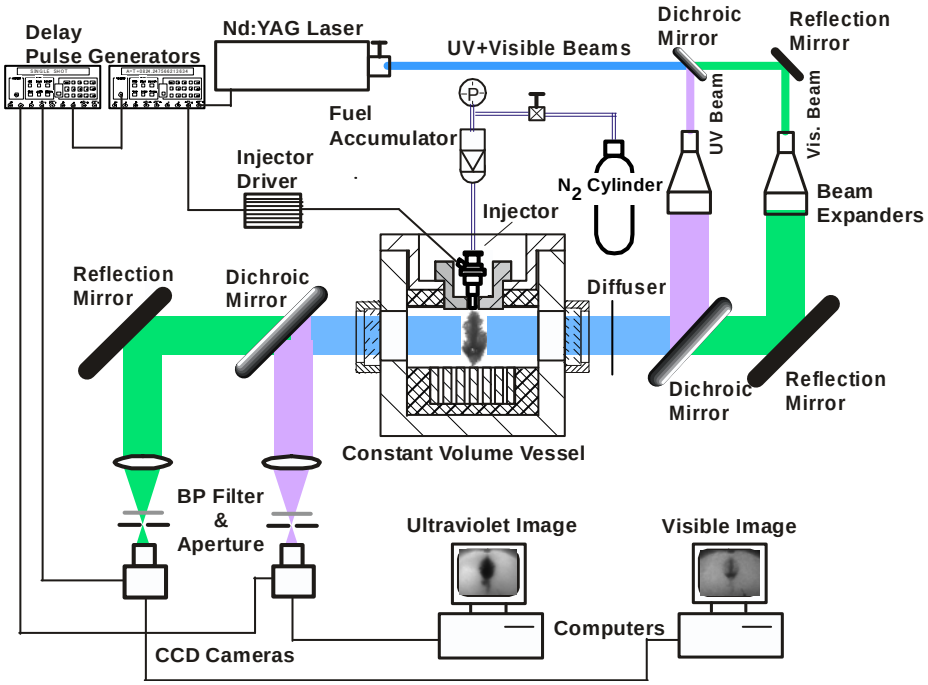

Fig. 3 Schematic of experimental apparatus for LAS measurement

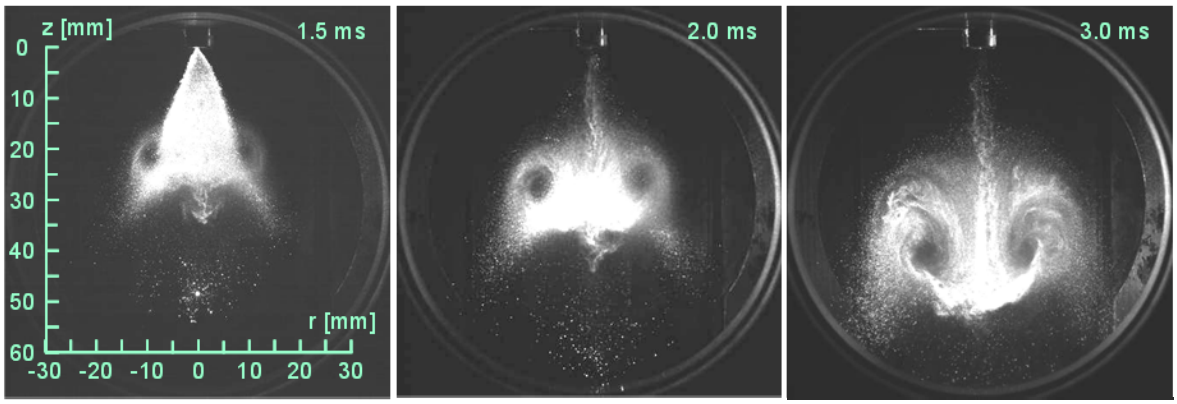

(a) P_a = 0.1 MPa

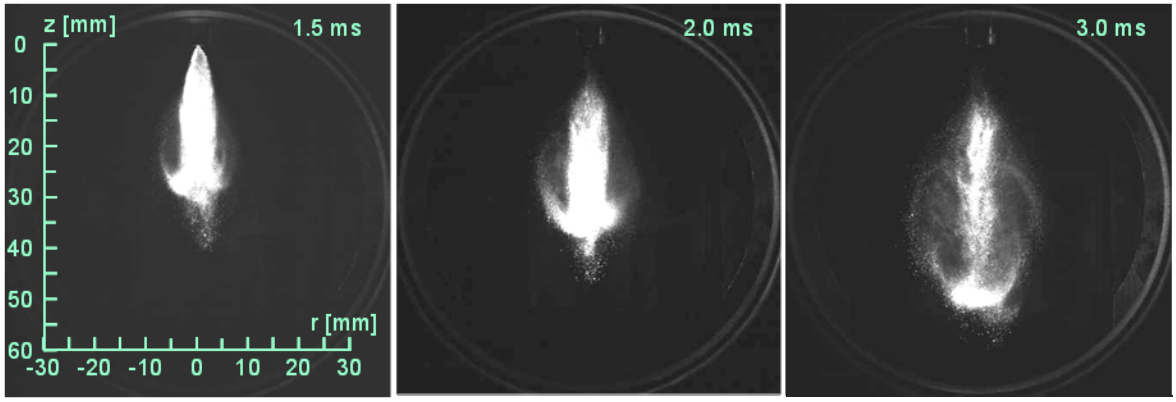

(b) P_a = 0.4 MPa

Fig. 4 Mie scattering images of spray droplets by laser sheet method (T_a = 300 K, Fuel: dry solvent)

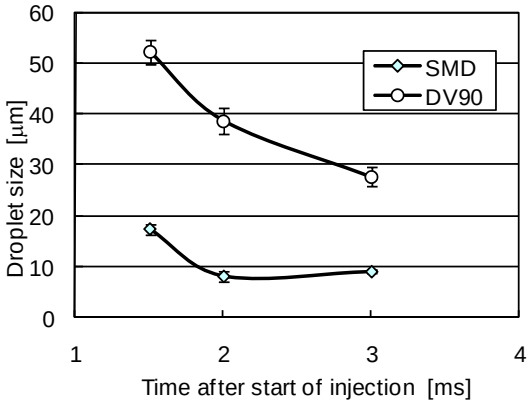

(a) P_a = 0.1 MPa

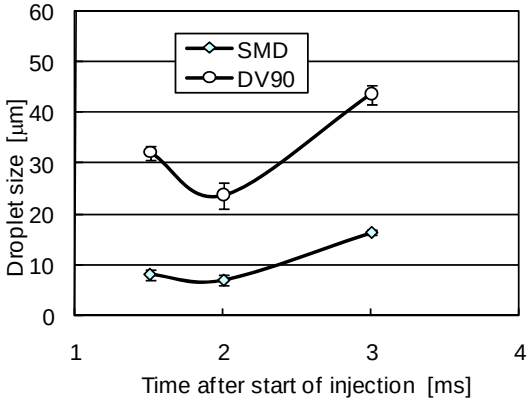

(b) P_a = 0.4 MPa

Fig.5 Temporal variations of SMD and DV90 (T_a = 300 K, Fuel: dry solvent, r = 0 mm, z = 30 mm)

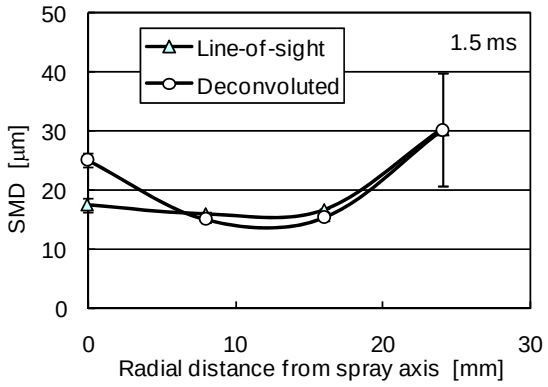

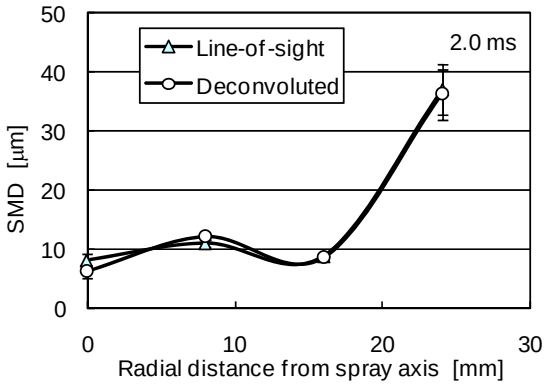

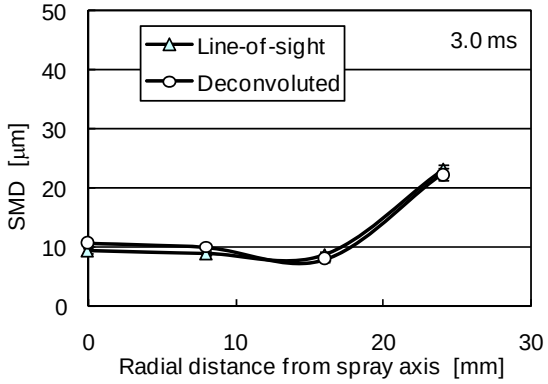

(a) P_a = 0.1 MPa

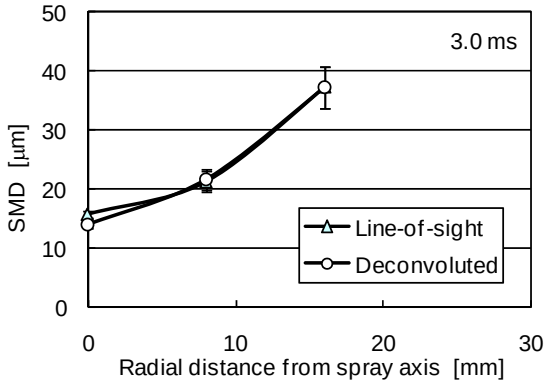

(b) P_a = 0.4 MPa

Fig.6 Spatial droplet size distribution (T_a = 300 K, Fuel: dry solvent, r = 0 mm, z = 30 mm)

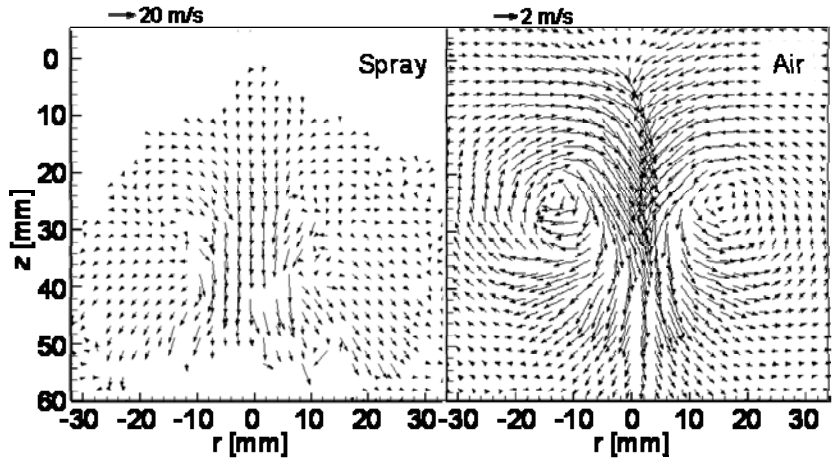

(a) P_a = 0.1 MPa

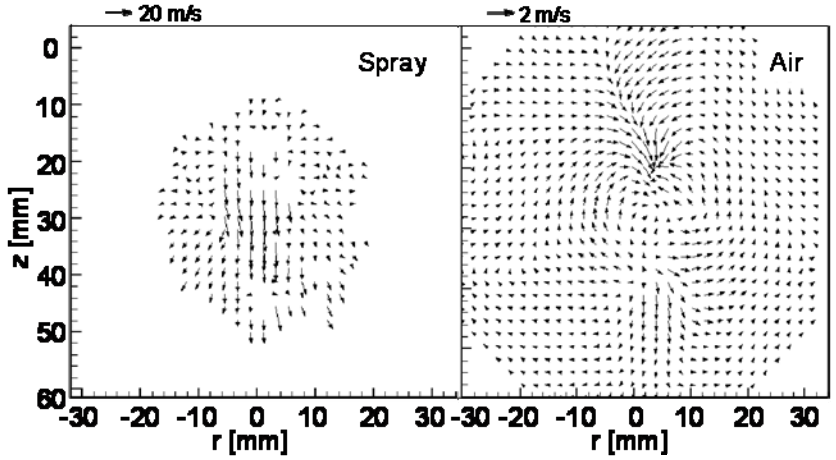

(b) P_b = 0.4 MPa

Fig. 7 Velocity distributions of spray droplets and spray-induced ambient air flow (T_a = 300 K, t = 3 ms ASOI, Fuel: dry solvent)

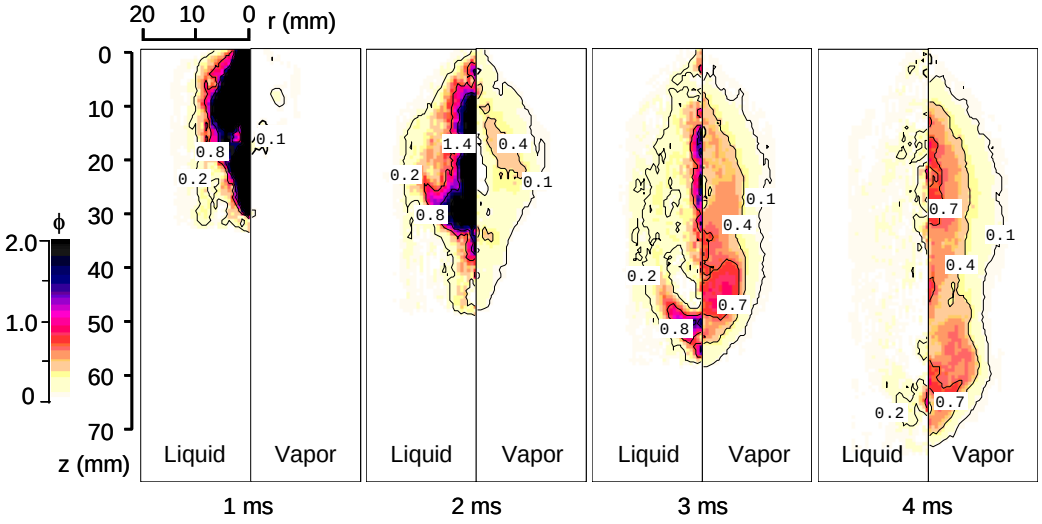

Fig. 8 Temporal variations of spatial equivalence ratio distributions of liquid and vapor phases in the spray (T_a = 500 K, P_a = 1.0 MPa, Fuel: p-xylene)

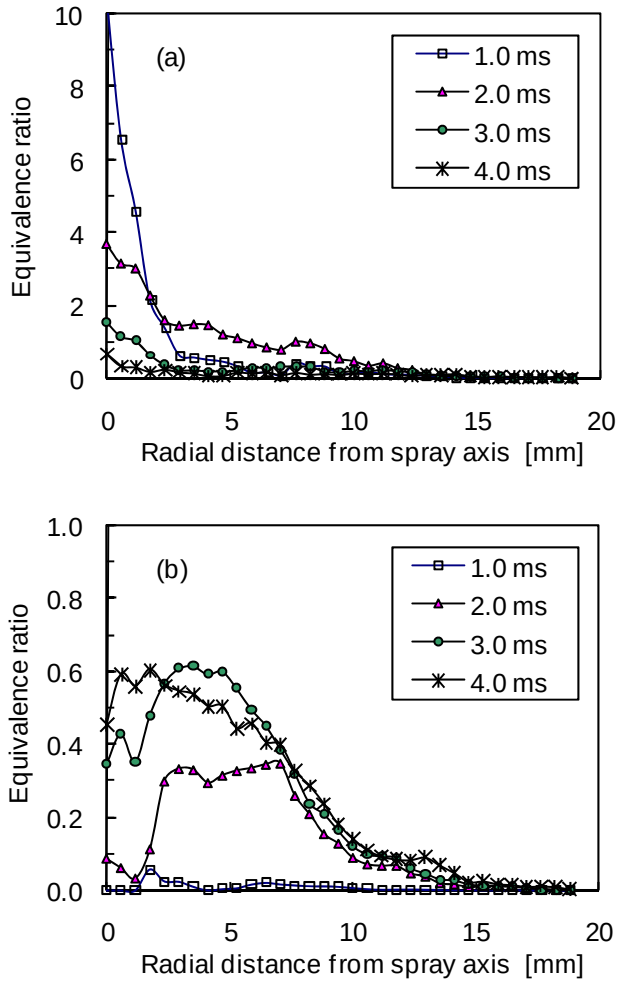

Fig. 9 Temporal variations of equivalence ratio distributions along radial direction from spray axis (T_a = 500 K, P_a = 1.0 MPa, Fuel: p-xylene, z=25 mm) (a) liquid phase; (b) vapor phase

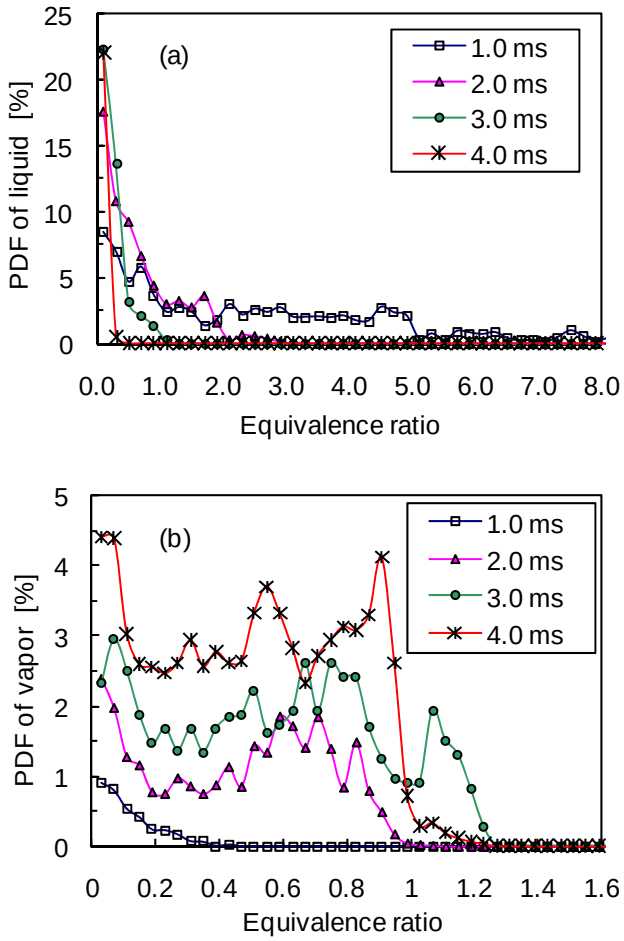

Fig. 10 Temporal variations of probability density function (PDF) of equivalence ratio in the (a) liquid and (b) vapor phase sprays (T_a = 500 K, P_a = 1.0 MPa, Fuel: p-xylene)

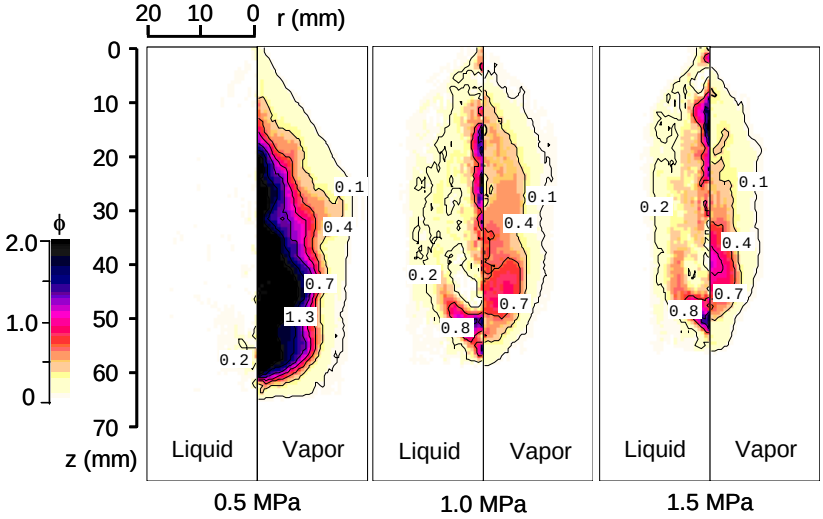

Fig. 11 Effect of ambient pressure on spatial equivalence ratio distributions of liquid and vapor phases in the spray (T_a=500 K, t = 3 ms ASOI, Fuel: p-xylene)

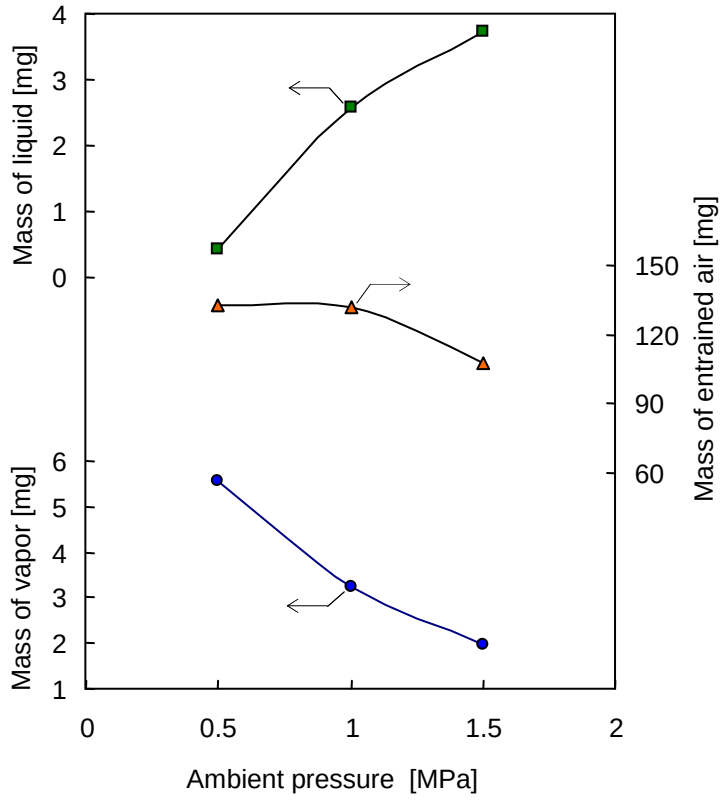

Fig. 12 Effect of ambient pressure on mass of liquid, vapor and entrained air in the spray (T_a=500 K, t = 3 ms ASOI, Fuel: p-xylene)